

Article

## A Critical Analysis of the Conventionally Employed Creep Lifting Methods

Zakaria Abdallah \*, Veronica Gray, Mark Whittaker and Karen Perkins

Institute of Structural Materials, College of Engineering, Swansea University, Swansea SA2 8PP, UK;  
E-Mails: v.a.gray@swansea.ac.uk (V.G.); m.t.whittaker@swansea.ac.uk (M.W.);  
k.m.perkins@swansea.ac.uk (K.P.)

\* Author to whom correspondence should be addressed; E-Mail: z.a.m.abdallah@swansea.ac.uk;  
Tel.: +44-1792-606-583; Fax: +44-1792-295-693.

Received: 9 December 2013; in revised form: 10 April 2014 / Accepted: 21 April 2014 /

Published: 29 April 2014

---

**Abstract:** The deformation of structural alloys presents problems for power plants and aerospace applications due to the demand for elevated temperatures for higher efficiencies and reductions in greenhouse gas emissions. The materials used in such applications experience harsh environments which may lead to deformation and failure of critical components. To avoid such catastrophic failures and also increase efficiency, future designs must utilise novel/improved alloy systems with enhanced temperature capability. In recognising this issue, a detailed understanding of creep is essential for the success of these designs by ensuring components do not experience excessive deformation which may ultimately lead to failure. To achieve this, a variety of parametric methods have been developed to quantify creep and creep fracture in high temperature applications. This study reviews a number of well-known traditionally employed creep lifting methods with some more recent approaches also included. The first section of this paper focuses on predicting the long-term creep rupture properties which is an area of interest for the power generation sector. The second section looks at pre-defined strains and the re-production of full creep curves based on available data which is pertinent to the aerospace industry where components are replaced before failure.

**Keywords:** creep; creep lifting methods; long-term creep behaviour; stress rupture; the Wilshire equations

---

## 1. Introduction

There are many applications where materials are required to operate for long periods in severe environments of high stresses and temperatures without failure. Examples of this are the power generation industry and the gas turbine sector where components are experiencing higher temperature environments as designers seek to increase thermal efficiency. Because of these harsh engineering environments, both areas are dependent on appropriate methods of creep lifing even though the specific requirements of each industry differ significantly. In the power generation sector, a significant part of the industry entails static parts experiencing pressure loads where creep is often the most critical damage mechanism. These plants are designed to operate for periods in excess of 100,000 h and often to 250,000 h, and, with vast amounts of material being required, it is clear there is an opportunity for significant cost savings through the employment of new alloys. However, working over such long timeframes means that it is not feasible to conduct 100,000 h creep tests on new materials in order to establish safe operating stresses for the life of the plant. Therefore, appropriate extrapolation methods are required in order to derive crucial design stress limitations from short term creep tests.

Many approaches to predicting creep have been proposed in an effort to infer long-term deformation behaviour. As such, parametric creep methods play a key role in design as they are essential in predicting the specific life of high temperature components [1,2]. Each of these approaches is a technique where short-term creep-rupture data can be extrapolated to longer-term scenarios using a time-temperature parameter. This concept is based on the assumption that all creep-rupture data for a given material can be combined to produce a single “master curve” where stress is mapped against a parameter that combines the effect of time and temperature. This can then be used to extrapolate to longer time frames such as those experienced in the power generation sector.

Contrastingly, for a gas turbine engines there are different design requirements due to the number of rotating parts which are more likely to fail from fatigue rather than creep. However, fatigue damage models rely on input stresses, which are dependent on stress relaxation, governed by creep deformation. Accurate creep models which describe creep strain evolution, particularly for relatively low creep strains, are therefore extremely desirable. Clearly, the goal of both industries is an all encompassing model capable of each of these requirements whilst being transferable across materials and providing confidence through supportive observations from experimental data. This is a goal which thus far has eluded engineers. Indeed, as recently as 2010 the extrapolation of creep data was rated as the most important challenge in the UK Energy Materials Strategic Research [3].

This paper critically reviews some of the most commonly used creep lifing methods available. It is structured with two themes; models capable of creep life extrapolation, and, models able to re-produce full creep curves based on limited creep data. Creep life extrapolation methods are evaluated using the National Institute of Materials Science (NIMS) creep data of a well-understood power generation alloy, Grade 22 Steel (2.25Cr-1Mo) [4]. Reproduction of creep curves from limited data is undertaken for the aerospace alloy Titanium 834. It should be noted that this paper is not an exhaustive review of all possible creep models but rather an overview and evaluation of the most commonly employed creep models. Previous studies have undertaken more thorough reviews of traditional methodologies providing guidance on acceptability criteria [5,6]. These criteria assisted in the assessment of methodologies explored in this paper prior to application of a mean squared error-based approach.

## 2. Approaches to Creep Life Predictions

Generally, the traditional approach to creep lifing has been based on a power law relationship between temperature,  $T$  and stress,  $\sigma$ . Arrhenius [1] relates these parameters to the creep rate through:

$$\dot{\epsilon}_s \propto \exp(-Q_c/RT) \quad (1)$$

and by Norton [1]:

$$\dot{\epsilon}_s \propto \sigma^n \quad (2)$$

where  $\dot{\epsilon}_s$  is the secondary or steady-state creep rate;  $Q_c$  is the activation energy for creep;  $n$  is the stress exponent and  $R$  is the gas constant. Combining these two relationships yields the basic power law Equation (1):

$$\dot{\epsilon}_s = A \cdot \sigma^n \cdot \exp(-Q_c/RT) \quad (3)$$

where  $A$  is a proportionality constant. The initial assumption when this law was introduced was that  $Q_c$  and  $n$  are constants. However, after further research, it was observed that these “constants” varied according to the imposed creep conditions and mechanisms involved in different stress and temperature regimes [7]. With pure metals, a decrease from  $n \cong 4$  to  $n \cong 1$  with decreasing stress, has been widely attributed to a change from diffusion-controlled dislocation processes to diffusional creep mechanisms not involving dislocation movement. However, at high stresses strengthened alloys with fine precipitate or insoluble particles can produce values of  $n \gg 4$  where the value for  $Q_c$  easily exceeds that of the activation energy for lattice diffusion,  $Q_{SD}$  [8]. No generally accepted interpretation has been agreed upon to account for these anomalously large  $n$  and  $Q_c$  values.

### 2.1. Traditional Power Law Creep Models

A wide variety of parametric approaches to creep lifing based on the above power law equation, Equation (3), have been developed over the past 60 years with varying degrees of success. A number of the most widely used power law approaches are explored in this section.

#### 2.1.1. The Larson-Miller Approach

This parametric method is one of the most widely employed techniques for stress-rupture behaviour prediction in metals. It was originally derived from the basic power law equation, Equation (3), by assuming a constant stress over a variable temperature range. The Larson-Miller approach is given by [9]:

$$P_{LM} = f(\sigma) = T \cdot (C_{LM} + \log t_f) \quad (4)$$

where  $C_{LM}$  and  $P_{LM}$  are the Larson-Miller constant and parameter, respectively.

Larson and Miller expanded their original proposal suggesting that the value of  $C_{LM}$  to be taken as 20 for metallic materials [9,10]. This presented a problem because if the value of  $C_{LM}$  is universally 20 for all metallic materials, then this implies that for the same testing conditions the time to fracture is the same for all metallic materials. In addition, this suggestion means that for a given material, once a set of stress-rupture curves at different temperatures are established, then over the

same temperature range these curves would be valid for any other material provided the stress scale is altered [11]. However, it was subsequently found that the value  $C_{LM}$  varies from one alloy to another and is influenced by factors such as cold-working, thermo-mechanical processing, phase transitions and/or other structural modifications [10]. To address this complexity,  $C_{LM}$  is a “fitted constant” acquired purely from the data with no physically meaningful description.

Although the Larson-Miller approach is widely used to model creep, it does have inherent limitations. Even though  $C_{LM}$  is given as a constant, it is known from observation that it is not constant for all conditions [7]. Furthermore, the parameters and constants described here have yet to be linked to any physical phenomena. Therefore, what the constants represent and how to predict them remains unclear, highlighting two common issues for many creep models. The first issue is that these empirical equations employ constants which upon investigation are often no longer constant over the conditions considered. The second is that the parameters used in the equations cannot be linked to any physical phenomena and hence, it is unclear what they represent. This means that it is difficult to expand such models to be able to extrapolate more widely and include factors such as cold-working, thermo-mechanical processing, phase transitions and/or other structural modifications known to change creep properties.

### 2.1.2. The Manson-Haferd Approach

Manson and Haferd [12] developed a linear time-temperature relationship for creep and stress-rupture data. This methodology was introduced in order to address the inaccuracy of the Larson-Miller approach resulting from the suggestion of a fixed  $C_{LM}$  for metallic materials [12,13]. The Manson-Haferd approach, like the Larson-Miller, assumes steady-state creep is dominated by power law behavior. However, the innovation of the Manson-Haferd approach assumes that the logarithm of the time varies linearly with temperature at a constant initial stress, according to [12,14]:

$$P_{MH} = f(\sigma) = (\log t - \log t_a)/(T - T_a) \quad (5)$$

where  $P_{MH}$ ,  $t_a$  and  $T_a$  are the Manson-Haferd parameter, time and temperature constants, respectively. The variable  $t$  refers either to the time to fracture,  $t_f$ , or, to a pre-defined strain level,  $t_e$ , and  $T$  is the absolute temperature of the creep test. Mapping iso-stress data as a function of time and temperature, *i.e.*,  $f(\sigma) = f(t, T)$  at  $\sigma = \text{constant}$ ,  $t_a$  and  $T_a$  are obtained from the intercepts of a linear fit, *i.e.*, at  $(t, T) \rightarrow (t_a, 0), (0, T_a)$ . This means that the Manson-Haferd parameter,  $P_{MH}$ , is composed of two constants unlike the Larson-Miller parameter,  $P_{LM}$ , which involves only one. The Manson-Haferd parameter,  $P_{MH}$ , can therefore be derived graphically from the point of intersection of the extrapolated iso-stress lines of  $\log t_f$  vs.  $T$ . Moreover, plotting  $P_{MH}$  vs.  $\sigma$ , forces all creep data to collapse onto a single “master curve” providing an equation that relates the stress to time and temperature [12].

The perceived advantage of this method over the Larson-Miller’s approach is that the parameter,  $P_{MH}$ , is composed of two constants relating time to temperature, thus, possibly giving this model better sensitivity to the time-temperature relationship. Once again, the physical meaning of  $t_a$  and  $T_a$  is not known and as such what they represent is unclear.

### 2.1.3. The Orr-Sherby-Dorn Approach

The Orr-Sherby-Dorn (OSD) [15] approach involves a time-temperature constant,  $C_{OSD}$ , based on the linear relationship of  $\log t$  vs.  $1/T$ . In the OSD approach, the initial premise of Larson and Miller has been modified such that the constant  $C_{LM}$  becomes a function of stress, and  $P_{LM}$  becomes a constant [13,14]. Based on these assumptions, the Larson-Miller relation, Equation (4), can be re-arranged to yield the Orr-Sherby-Dorn equation [15]:

$$P_{OSD} = f(\sigma) = \log t_f - C_{OSD}/T \quad (6)$$

where  $P_{OSD}$  and  $C_{OSD}$  are the Orr-Sherby-Dorn parameter and constant, respectively. This method offers a different perspective on the relationship between parameters and constants which leads to it producing smooth creep curves rather than sigmoidal ones. This distinction in the curve shape is one reason the OSD method may produce better creep rupture predictions than other methods.

Once again, this approach suffers from its empirical nature. Similar to the Larson-Miller and Manson-Haferd approaches, the OSD utilises a constant,  $C_{OSD}$ , based on  $Q_c$  which is usually obtained from sparse data [15]. The effect of this is that any variation in  $Q_c$  will consequently ensure that the superimposed parametric plots will be non-linear [16]. Indeed, there is evidence that in some cases, creep activation energy appears to systematically increase through the primary creep region [17]. The variation in the value of  $C_{OSD}$  has been observed experimentally by Murray and Truman [18]. Given that  $C_{OSD}$  is the gradient of  $\log t_f$  vs.  $1/T$ , it was proposed by OSD that the adjacent  $\log \sigma$  vs.  $\log t_f$  curves will be equidistant from each other along the time scale [11]. In principle, this approach can be used by obtaining  $C_{OSD}$  from a single plot, but in reality,  $C_{OSD}$  is usually an average value obtained from a number of  $\log t_f$  vs.  $1/T$  values.

### 2.1.4. The Manson-Succop Approach

The Manson-Succop approach [19] describes the iso-stress values to be proportional to  $\log t_f$  and  $T$ . This differs from OSD method which relates the iso-stress data to  $\log t_f$  and  $1/T$ . The Manson-Succop parameter and constant,  $P_{MS}$  and  $C_{MS}$ , are related by [19]:

$$P_{MS} = f(\sigma) = \log t_f + C_{MS} \cdot T \quad (7)$$

This approach produces similarly shaped curves to the OSD approach, however, differs in its method of describing the time-temperature relationship. This method was reviewed by Zharkova and Botvina [20] who confirmed that during long-term creep tests, fracture mechanisms changed according to the applied stress and the loading time. Although the mechanism changed, it was concluded that the derived constant did not change for the Manson-Succop, Larson-Miller or Manson-Haferd approaches. In the opinion of these authors [20], this claim has not been definitively adopted as there is evidence to both support and counter the idea that the constants in these approaches are independent of the creep mechanism.

### 2.1.5. The Goldhoff-Sherby Approach

This approach is similar to the Manson-Haferd method with the difference being that the constructed iso-stress lines will converge to a point  $(1/T_a, t_a)$  such that [21]:

$$P_{GS} = f(\sigma) = (\log t - \log t_a)/(1/T - 1/T_a) \quad (8)$$

where  $t_a$  and  $T_a$  are the time and temperature constants, respectively. The mathematical procedures are similar to those applied using the Manson-Haferd approach, however,  $\log t_f$  is plotted against  $1/T$  at constant stresses with the slope being the value of the Goldhoff-Sherby parameter,  $P_{GS}$ . An average value for  $\log t_a$  and  $1/T_a$  should then be chosen in order to construct the stress vs. time to fracture curves. This model contains the potential time-temperature sensitivity of the Manson-Haferd but offers a slightly different curve shape.

### 2.1.6. The Soviet Prediction Approach

This method can be described by two models; Soviet models (1) and (2), given by [22,23]:

$$\text{Soviet Model (1): } \log t = a + b \log T + c \log \sigma + d/T + f \cdot \sigma/T \quad (9)$$

$$\text{Soviet Model (2): } \log t = a + b \log T + c \log(\sigma/T) + d \cdot \sigma/T + f/T \quad (10)$$

where  $a$ ,  $b$ ,  $c$ ,  $d$  and  $f$  are constants to be determined from fitting the equations to data. This method uses a large number of constants which allows for greater sensitivity, but the constants are not easily separable from the variables  $T$  and  $\sigma$ , meaning that multiple constants need to be fitted simultaneously. This might result in more than one possible set of values for  $a$ ,  $b$ ,  $c$ ,  $d$  and  $f$ . From the experience of the authors of this paper, fitting constants can lead to unphysical curves and this should be noted when employing this method. A means of fitting these multiple constants simultaneously is provided by the software PD6605 which iterates the numerical coefficients of each equation, first to optimise their values and then to determine which has the greatest likelihood of providing the most accurate results [24]. Evans [22] expressed that Soviet Model (1) was highly effective in modeling the known rupture times, but was totally inadequate for predicting beyond the range of input data. However, this inability to generalise or the tendency to overfit the interpolative data set, is a characteristic of all parametric techniques [22].

### 2.1.7. The Minimum Commitment Approach

This method was proposed by Manson and Ensign [25,26] in an effort to give larger flexibility to parametric analysis of creep data. In addition, it was proposed as a way to unite conflicting approaches into a single equation with sufficient generality. The Minimum Commitment approach is given by [25,26]:

$$\log t = a + b \log \sigma + c \cdot \sigma + d \cdot \sigma^2 + f/T + g/T \quad (11)$$

In the above equation there are six constants that need to be determined via regression analysis. Similar to the Soviet approach, the large number of constants coupled to variables introduces analysis issues when performing any fitting process but gives greater detail and sensitivity to the time-temperature-stress relationship. Among those who have studied this methodology was Jow-Lian Ding *et al.* [27] who found that the results of regression analyses indicated that the Minimum Commitment model fitted the creep data studied only slightly better than the Larson-Miller model regardless of the high number of constants.

## 2.2. Modern Creep Lifting Approaches

### 2.2.1. The Hyperbolic-Tangent Approach

Developed by Rolls-Royce plc (London, UK) in the 1990s for creep strain and life predictions, this approach implements the idea that the highest stress that can be applied to a specified material at a certain creep temperature is the ultimate tensile strength,  $\sigma_{TS}$ , of the material. The stress rupture behaviour is described by hyperbolic tangent curves over a wide range of temperatures, such that [28–30]:

$$\sigma = \sigma_{TS}/2 \{1 - \tanh[k \cdot \log(t/t_i)]\} \quad (12)$$

where  $k$  and  $t_i$  are fitting parameters that can be obtained via regression analysis by plotting at constant temperatures,  $\tanh^{-1}(1 - 2(\sigma/\sigma_{TS}))$  vs.  $\log t_f$ . Once these values are obtained, they can then be inserted into Equation (12) to produce the stress rupture curves. The inflection point of these curves at  $\sigma = 0.5\sigma_{TS}$  provides a different shape to that of the previous methods and therefore may provide a better fit for creep data with changes in mechanism that significantly impact creep lifetime.

### 2.2.2. The Wilshire Approach

Developed at Swansea University by Wilshire [16,31], this methodology has been applied widely for long-term creep predictions [16,31]. The innovation of this method is that the stress applied is normalised by the ultimate tensile strength,  $\sigma_{TS}$ . The stress can also be normalised by the yield stress,  $\sigma_y$ , however, the obtained data fit is generally less accurate as the value of  $\sigma_y$  is more difficult to be precisely measured than the  $\sigma_{TS}$  [32]. Normalisation by the  $\sigma_{TS}$  also provides the advantage of values of  $(\sigma/\sigma_{TS})$  being between 0 and 1, meaning that property comparisons for different metals and alloys can be significantly simplified [31].

Normalising the applied stress in the power law equation,  $\dot{\epsilon}_m = A \cdot \sigma^n \cdot \exp(-Q_c/RT)$ , and defining the minimum creep rate,  $\dot{\epsilon}_m$ , as in the Monkman-Grant relationship,  $\dot{\epsilon}_m = M/t_f$ , gives [16]:

$$\dot{\epsilon}_m = M/t_f = A^* \cdot (\sigma/\sigma_{TS})^n \cdot \exp(-Q_c^*/RT) \quad (13)$$

where  $A^* \neq A$  and  $Q_c^* \neq Q_c$ . In this case,  $Q_c^*$  is determined from the temperature dependence of  $\dot{\epsilon}_m$  and/or  $t_f$  at constant  $(\sigma/\sigma_{TS})$ , unlike  $Q_c$  which is normally calculated at constant  $\sigma$ . As it stands, this equation does not permit reliable extrapolation of the short-term measurements due to the unpredictable fall in  $n$  values as  $(\sigma/\sigma_{TS})$  decreases. However, Equation (13) reduces the scale and the number, but not the maximum duration, of experimental tests needed to be undertaken to obtain long-term strength data [16,31].

Since  $\sigma_{TS}$  represents the maximum stress that can be applied on a material at a specific creep temperature, the data sets can be described over the entire stress range from  $(\sigma/\sigma_{TS}) = 1$  to  $(\sigma/\sigma_{TS}) = 0$ . In addition, it is evident that  $\dot{\epsilon}_m \rightarrow \infty$  and  $t_f \rightarrow 0$  as  $(\sigma/\sigma_{TS}) \rightarrow 1$ , whereas  $\dot{\epsilon}_m \rightarrow 0$  and  $t_f \rightarrow \infty$  when  $(\sigma/\sigma_{TS}) \rightarrow 0$ . These essential criteria are met by augmenting Equation (13) so that the stress and temperature dependences of the creep life are described by [16,31,32]:

$$\sigma/\sigma_{TS} = \exp(-k_1 [t_f \exp(-Q_c^*/RT)]^u) \quad (14)$$

where the values of the coefficients  $k_1$  and  $u$  are fitting constants. To obtain  $k_1$  and  $u$ , a linear fit of  $\log(t_f \exp(Q_c^*/RT))$  vs.  $\log(-\log(\sigma/\sigma_{TS}))$  is produced with gradient equal to  $u$ , and, intercept equal to  $\log k_1$ .

This method, unlike the others, produces more physically realistic curves as  $\dot{\epsilon}_m \rightarrow \infty$  and  $t_f \rightarrow 0$  when  $(\sigma/\sigma_{TS}) \rightarrow 1$ , and  $\dot{\epsilon}_m \rightarrow 0$  and  $t_f \rightarrow \infty$  when  $(\sigma/\sigma_{TS}) \rightarrow 0$ . It also has only two fitting constants easily determinable from limited data that remain conditionally constant. This statement means that when plotting to obtain  $k_1$  and  $u$ , it has been observed that up to two linear regimes are sometimes obtained, referred to as the high and low stress regimes. This means that  $k_1$  and  $u$  may have different values above and below a certain normalised stress threshold thought to arise from a change in creep mechanism. Although this change in constants has been observed,  $k_1$  and  $u$  in their respective high and low stress regimes have so far proven to be constant.

### 3. Approaches to Reproducing Full Creep Curves

In the same manner in which stress-rupture prediction has been approached, this section considers approaches for creep strain predictions and hence the prediction of full creep curves. As stated previously, this study investigates only a small number of available methods, focusing mainly on more recently published techniques. The ECCC report published in 2003 provides a more extensive review of these and other methods [33].

#### 3.1. The $\theta$ -Projection Approach

The principle of the  $\theta$ -Projection approach is that creep curves under uniaxial constant stress measured over a range of stresses and temperatures can be “projected” to other stress/temperature conditions re-constructing full creep curves. The required properties can then be read off the newly constructed curves [34]. The  $\theta$ -Projection concept in its most general form is the 4- $\theta$  equation [35]:

$$\varepsilon = \theta_1[1 - \exp(-\theta_2 \cdot t)] - \theta_3[1 - \exp(\theta_4 \cdot t)] \quad (15)$$

where  $\theta_1$  and  $\theta_3$  are “scaling” parameters that define the extent of the primary and tertiary creep with respect to strain. Whereas  $\theta_2$  and  $\theta_4$  are “rate” parameters characterising the curvature of the primary and tertiary creep curves [36,37]. This method has been found to provide quite poor fits to experimental creep data for small strain values [35]. Deviations from experimental creep measurements were also found particularly in the late tertiary stage by Evans and Wilshire [37] when this method was used. In response to these deviations, a modification was suggested by Evans [38] to improve the fit at very small strain values. This has been achieved by adding another two extra parameters to Equation (15) to produce 6- $\theta$  equation [38]:

$$\varepsilon = \theta_1[1 - \exp(-\theta_2 \cdot t)] - \theta_3[1 - \exp(\theta_4 \cdot t)] + \theta_5[1 - \exp(-\theta_6 \cdot t)] \quad (16)$$

In this equation, the first two terms have the same physical meaning as in Equation (12). The additional third term describes the early primary creep behaviour that results from initial sliding relaxation across grain boundaries [36]. According to Evans [35,36,38], this modified equation provided better results when applied to creep data.

#### 3.2. The Uniaxial Creep Lifting Approach

This deformation mechanism-based approach was recently developed at Rolls-Royce Canada by Wu [38] in an effort to describe the entirety of creep strain curve *vs.* time. It considers that creep



deformation occurs by grain boundary sliding (GBS), dislocation glide (DXNG), dislocation climb (DXNC) and diffusion (DFN) mechanisms such that for a polycrystalline material, the total strain rate,  $\dot{\epsilon}$ , is equal to the sum of the contributions from each mechanism [39]:

$$\dot{\epsilon} = \dot{\epsilon}_{\text{gbs}} + \dot{\epsilon}_{\text{g}} + \dot{\epsilon}_{\text{c}} \quad (17)$$

Re-arranging this equation and expressing the strain rate,  $\dot{\epsilon}$ , in terms of strain,  $\epsilon$ , gives [39]:

$$\epsilon = \epsilon_0 + \epsilon_p [1 - \exp(-t/t_{\text{tr}})] + 1/M [\exp(M \cdot k \cdot t) - 1] \quad (18)$$

The primary strain,  $\epsilon_p$ , is obtained from the linear projection of the secondary/steady-state region of the creep curve at  $t = 0$ . The transient time,  $t_{\text{tr}}$ , is defined as the transition point from primary to secondary/steady-state creep. The slope  $k$  corresponds to the minimum creep rate and  $M$  is a factor obtained from the slope of  $\log \dot{\epsilon}$  against  $t$ . For creep curve analysis, one needs to extract the creep curve parameters,  $\epsilon_p$ ,  $t_{\text{tr}}$ ,  $k$  and  $M$  from actual creep strain vs. time curves and then apply Equation (18) to predict the creep strain accumulation (see [39]). The parameters in Equation (18) can be expressed in terms of stress and  $\sigma_{\text{TS}}$  such that:

$$t_{\text{tr}}, k \text{ and } M = f(\sigma/\sigma_{\text{TS}}) \quad (19)$$

$$\epsilon = \epsilon_0 + \epsilon_p f(\sigma/\sigma_{\text{TS}}, t) \quad (20)$$

The advantage of this approach is that once the parameters are expressed in terms of  $\sigma$  and  $\sigma_{\text{TS}}$  at a given temperature, Equation (18) can then be used to construct full creep curves at any specified stress for that temperature. In other words, only few tests are required at a given temperature to obtain the relationship, *i.e.*,  $f(\sigma/\sigma_{\text{TS}})$ , and the unknown parameters from which a database of creep curves can be generated at any given stress level outside the experimentally investigated range.

### 3.3. The Wilshire Approach

In addition to the ability to describe the stress-rupture behaviour, this technique has been extended to accurately re-construct full creep curves [40]. The time to fracture,  $t_f$ , in Equation (14) can be replaced by the time to a pre-defined strain level,  $t_\epsilon$ , which yields [16,31,40–42]:

$$\sigma/\sigma_{\text{TS}} = \exp(-k_3 [t_\epsilon \cdot \exp(-Q_c^*/RT)]^w) \quad (21)$$

where  $k_3$  and  $w$ , are constants to be determined following the similar process previously described. It was found elsewhere [40] that the value of  $w$  and  $k_3$  used in Equation (21) is independent of stress and temperature at any selected strain level and thus they can be expressed over a range of selected strains such that:

$$w = f_1(\epsilon) \quad (22)$$

$$k_3 = f_2(\epsilon) \quad (23)$$

Inserting these two expressions into Equation (21) gives:

$$\sigma/\sigma_{\text{TS}} = \exp(-f_2(\epsilon) \cdot [t_\epsilon \cdot \exp(-Q_c^*/RT)] f_1(\epsilon)) \quad (24)$$

Re-arranging this equation yields an equation that relates the strain,  $\epsilon$ ; to stress,  $\sigma$ ; temperature,  $T$ ; over time,  $t$ , such that:

$$\epsilon = f(t, \sigma, T) \tag{25}$$

Obtaining Equation (25) means that full creep curves at various stresses and temperatures can be re-constructed.

### 4. Results

This section is divided into two parts, namely; those for the creep life prediction approaches, and, those for full creep curve representation. In the first section, the material used is Grade 22 Steel whereas for full reproduction of creep curves Titanium IMI834 creep data was employed. Grade 22 steel was selected for this review as it is a widely used material with data covering appropriate creep lives and also because it is a difficult material to effectively life, aiding in exposing limitations of the approaches assessed here. Similarly, Titanium 834 has been selected as the model material due to its wide employment in the aerospace industry, in particular the compressor of gas turbine aeroengines. The reasons for this selecting Titanium 834 are the relevance of this material to the aerospace industry and the availability of creep data.

#### 4.1. Grade 22 Steel Data

As already noted, the values of  $Q_c$  and  $n$  are important when studying creep properties. The creep data of Grade 22 Steel was obtained from the National Institute of Materials Science (NIMS). Figure 1a depicts the exponent  $n$  at various conditions whereas Figure 1b shows the value of  $Q_c$  at various conditions. From these two plots, it is evident that both  $n$  and  $Q_c$  are not constants under the investigated conditions which implies that any involvement of such constants in the parametric approaches will ensure inaccuracies in their predictions.

**Figure 1.** The calculation of the: (a) stress exponent  $n$ ; (b) the activation energy  $Q_c$  at various conditions for Grade 22 Steel.

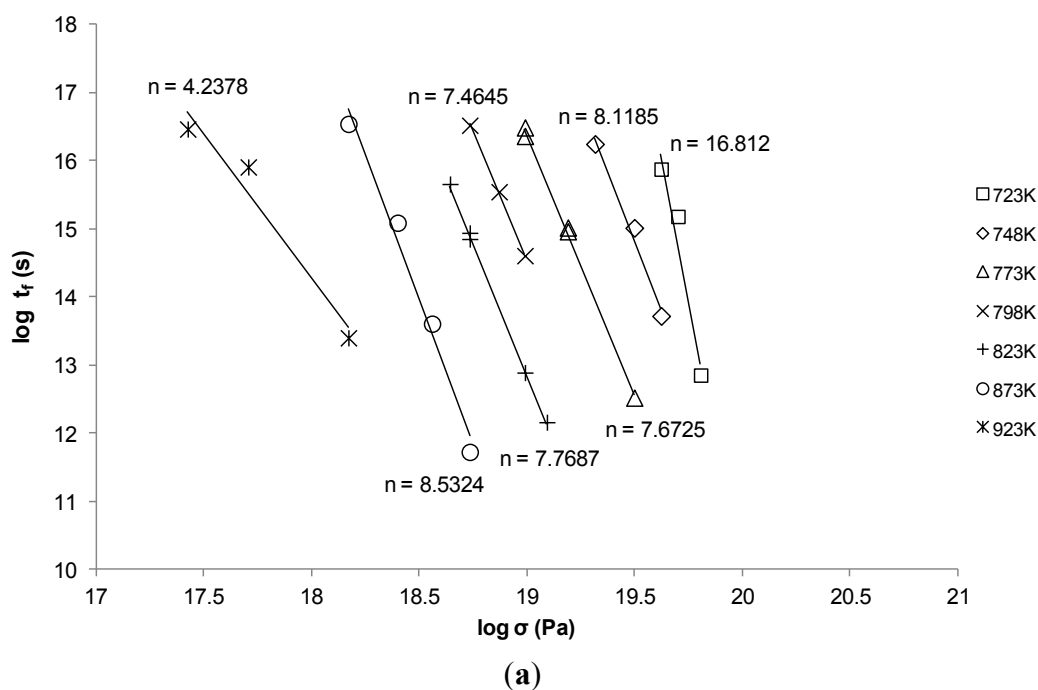
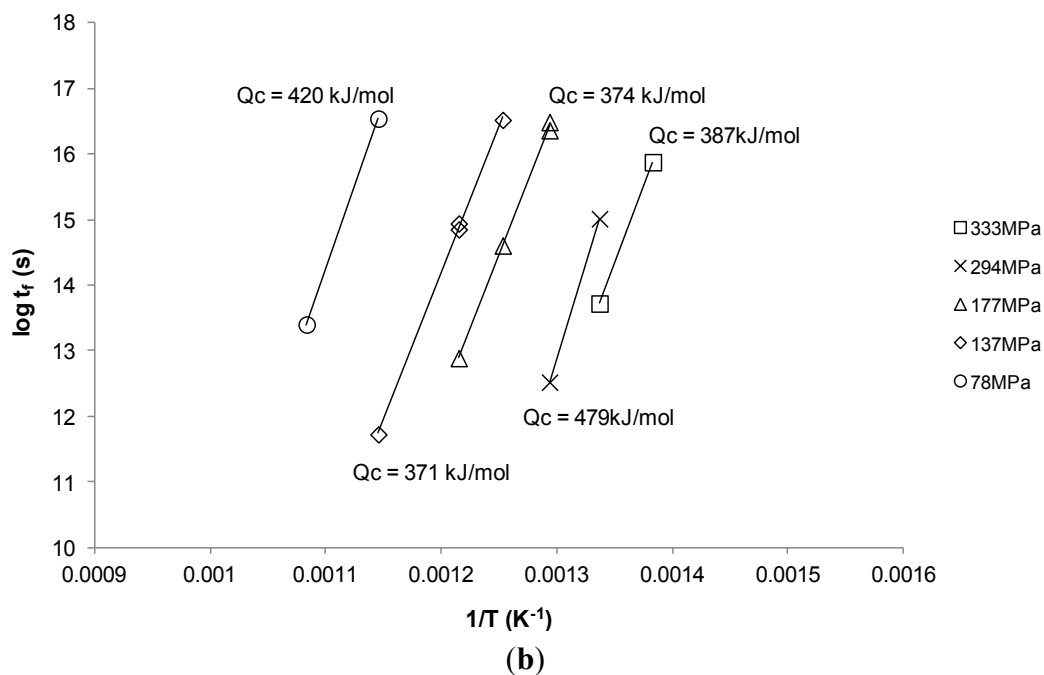


Figure 1. Cont.



#### 4.2. Titanium IMI834 Data

An extensive matrix of creep testing has been carried out at Swansea University using Uniaxial constant-stress creep machines performed in air according to ISO 204:2009 [43] on this material. The alloy IMI834 is widely used in the rings, compressor discs and blades for gas turbines and jet engine applications [44]. The results of these creep tests are used here for reconstructing full creep curves utilising the various approaches.

#### 4.3. Creep Life Predictions (Steel 22 NIMS Creep Data)

In each creep lifing predictive approach explored, data of stress rupture lives <5000 h was used to determine the constants and parameters for each approaches and then applied to the larger complete dataset. In each of the following figures experimental values are represented as “points” and creep rupture model predictions are shown as “solid lines”.

##### 4.3.1. The Larson-Miller Approach

Using the Larson-Miller approach,  $\log t_f$  vs.  $1/T$  was plotted at constant stress with the value of  $C_{LM}$  assumed constant although observed otherwise [14,16,45]. Predicted curves based on <5000 h data are shown alongside the available NIMS data in Figure 2.

The fits in Figure 2 are considered reasonable for the lower temperatures. As the temperature increases, the model flattens out and no longer reflects the shape or trend of the measured data. This supports the idea that the Larson-Miller model was developed based on low temperature deformation results making extrapolation at the high temperatures inaccurate [46].

### 4.3.2. The Manson-Haferd Approach

Figure 3 shows the application of the Manson-Haferd approach. This fit shows a similar sigmoidal shape to Larson-Miller but with a substantially worse fit in this case. From Figure 3, it can be observed that the best fits are obtained at the intermediate temperatures. For the extreme temperatures, *i.e.*, 723 and 923 K, the Manson-Haferd model fails to predict the experimental results. The exaggerated sigmoidal and flat shapes at 723 and 923 K, respectively, mean that the curves are unable to describe the actual creep properties at these conditions.

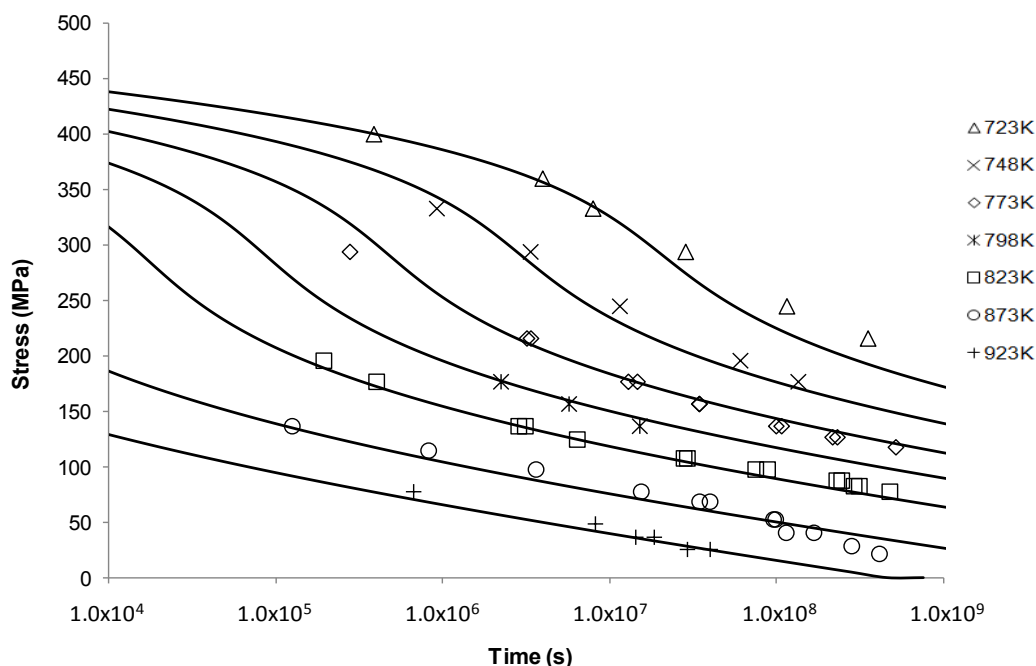
### 4.3.3. The Orr-Sherby-Dorn Approach

The OSD predictive curves are shown in Figure 4. This approach, unlike the previous ones, produced a smooth decaying curve. From these results it can be seen that this curve shape fits well with the longer life data at lower temperatures. It no longer provides a good fit for higher temperature data, nor the shorter rupture lives possibly due to changes in creep mechanism.

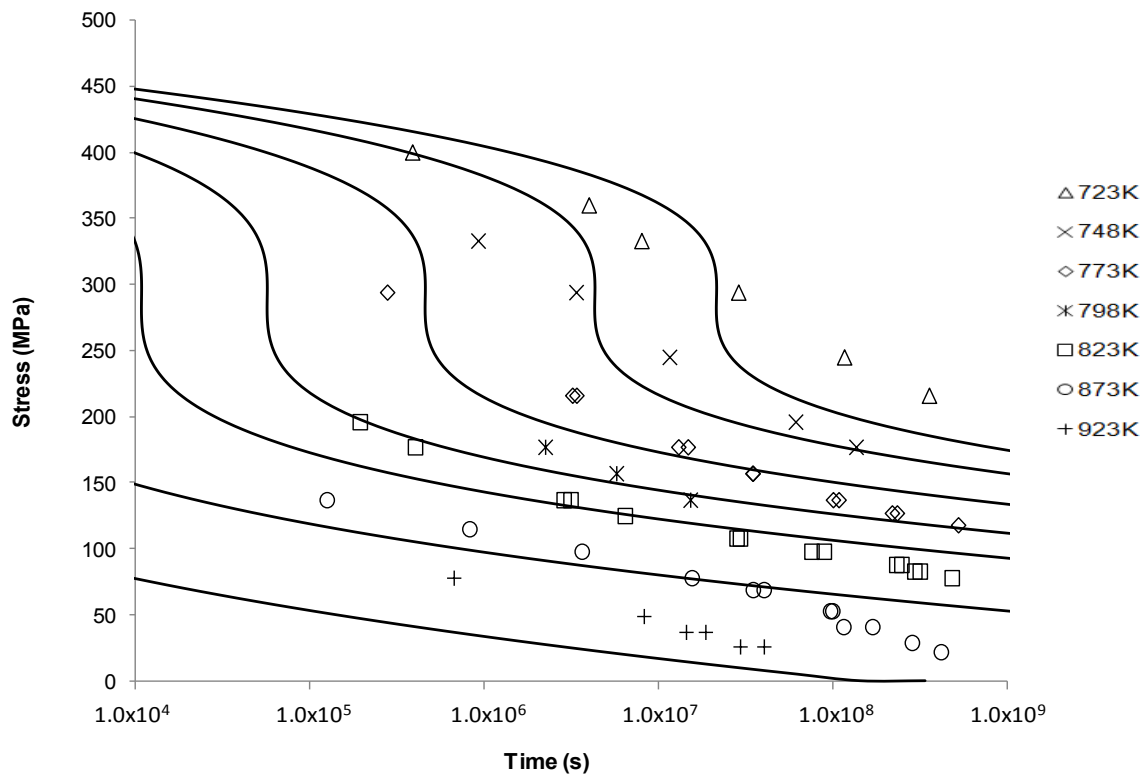
### 4.3.4. The Manson-Succop Approach

Figure 5 shows the results of applying the Manson-Succop approach to predicting creep rupture time. This method produced a similar creep curve shape to OSD shown in Figure 4. This is to be expected as these two methods are very similar with the difference between them lying in the time-temperature relationship ( $T$  vs.  $1/T$ ). However, this approach provides the best fit for creep rupture data at the intermediate temperatures and intermediate lifetimes.

**Figure 2.** The Larson-Miller’s stress vs. time to fracture predictive curves using Grade 22 Steel creep data.



**Figure 3.** The Manson-Haferd's stress vs. time to fracture predictive curves using Grade 22 Steel creep data.



**Figure 4.** The Orr-Sherby-Dorn's stress vs. time to fracture predictive curves using Grade 22 Steel creep data.

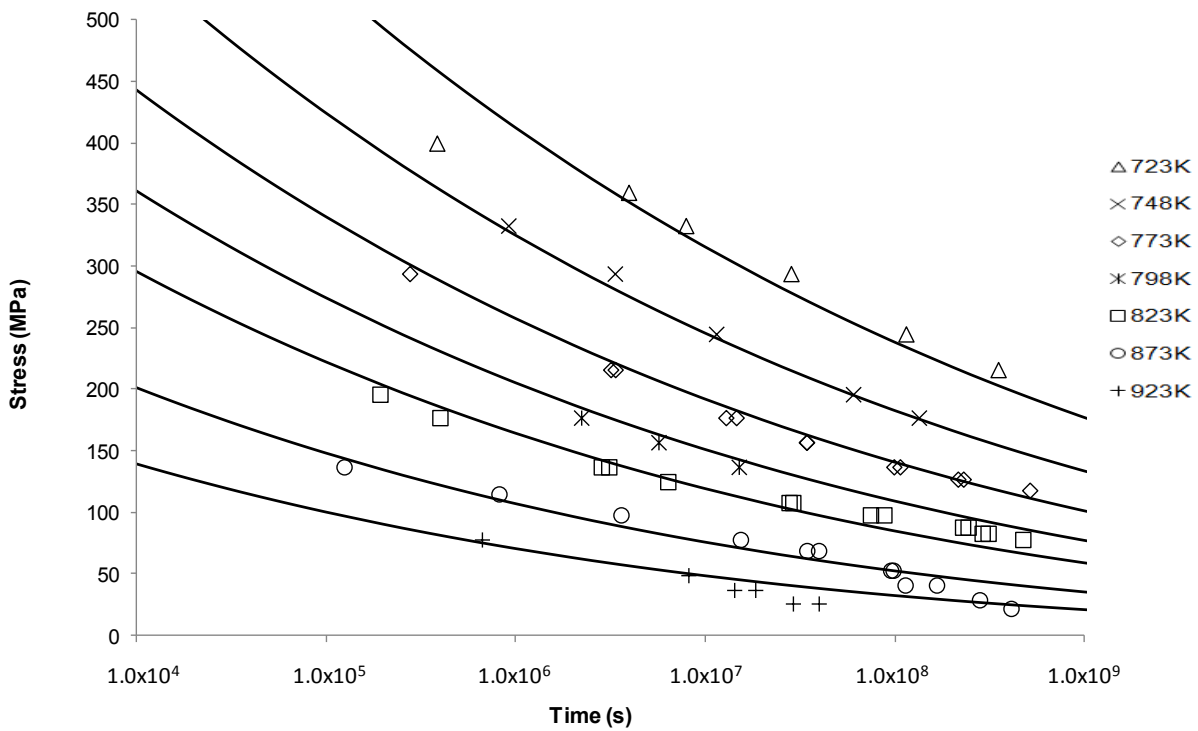
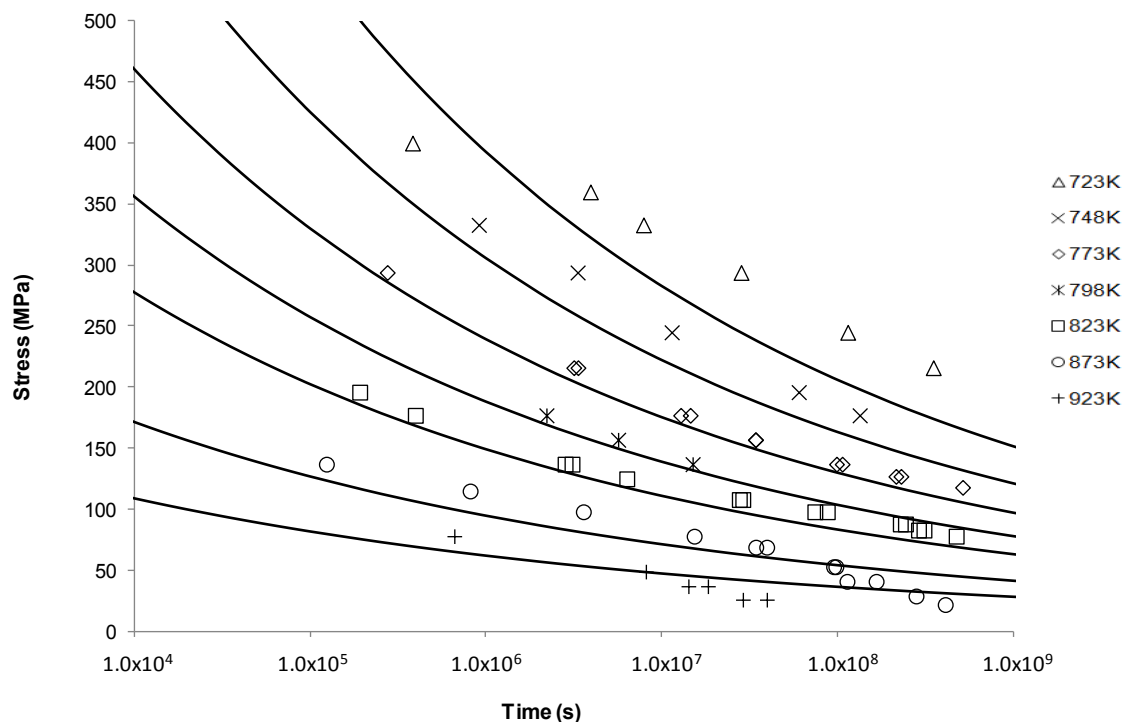


**Figure 5.** The Manson-Succop's stress vs. time to fracture predictive curves using Grade 22 Steel creep data.



#### 4.3.5. The Goldhoff-Sherby Approach

This approach, shown in Figure 6, produced similar results to the Manson-Haferd approach in Figure 3. The similarity of methods arises from their form with the difference arising from each approach's time-temperature relationship ( $T$  vs.  $1/T$ ). Unlike the Manson-Haferd method, the Goldhoff-Sherby approach produces better fits to the experimental data with its best fits in the intermediate to high temperatures, long and very short lifetime range.

The above models are considered the most simplistic of those reviewed in this paper. It can be seen that they do not provide good fits to experimental data, and as such, are often implemented in a more flexible way. The more practical application of these models provides individual fits at each temperature such that their parameters function,  $P$ , change with temperature rather than being tied to an initially derived value [47–49]. This produces substantially better fits but also introduces the unknown dependency of these parameters, and hence constants, to temperature. It also means more tests need to be done in order to satisfy the minimum statistical threshold as each temperature is effectively a new “unique” set of data.

#### 4.3.6. The Soviet Prediction Approach

Figures 7 and 8 depict the predictive curves of the Soviet Prediction approach. Both Soviet 1 and Soviet 2 produced very flat  $\sigma$  vs.  $t$  curves that did not reflect the trend of the data. This is demonstrative of the point made by Evans [22] that extrapolation beyond the input data using these models was found to be highly inaccurate possibly due to the model not replicating the trending behaviour.

**Figure 6.** The Goldhoff-Sherby’s stress vs. time to fracture predictive curves using Grade 22 Steel creep data.

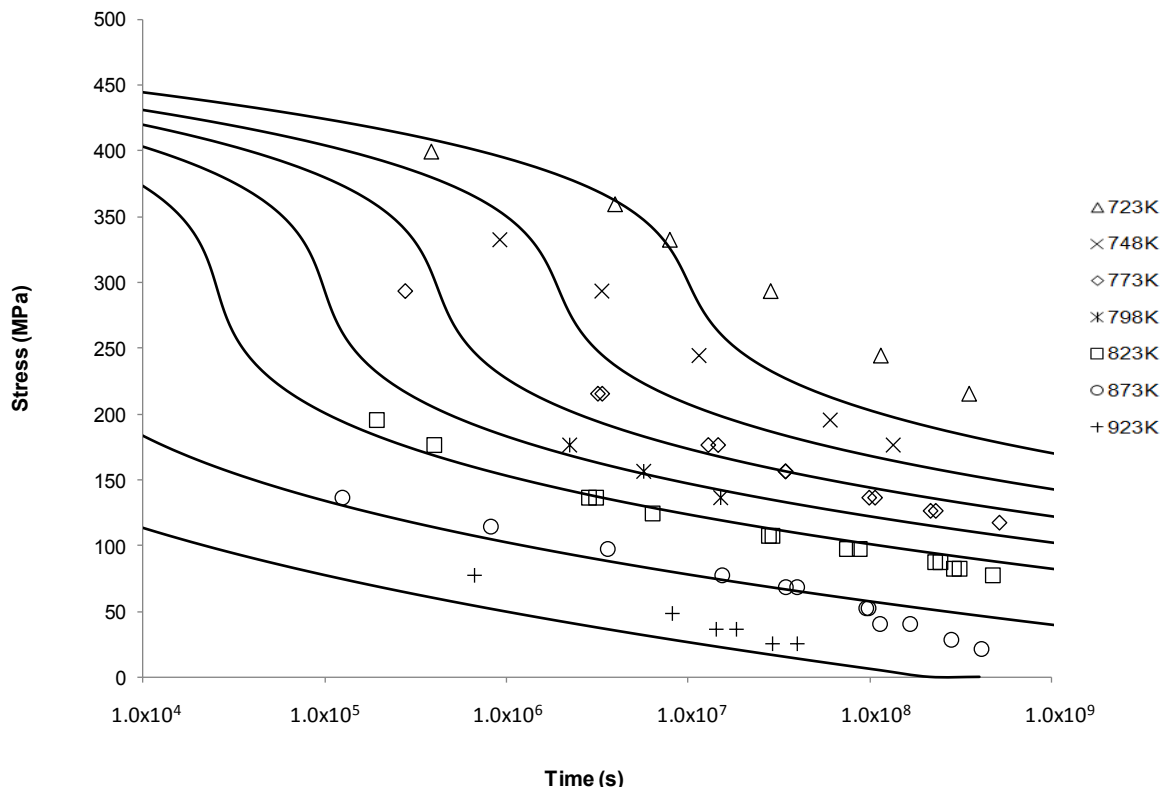


**Figure 7.** The stress vs. time to fracture curves of Soviet Model 1 using Grade 22 Steel creep data.

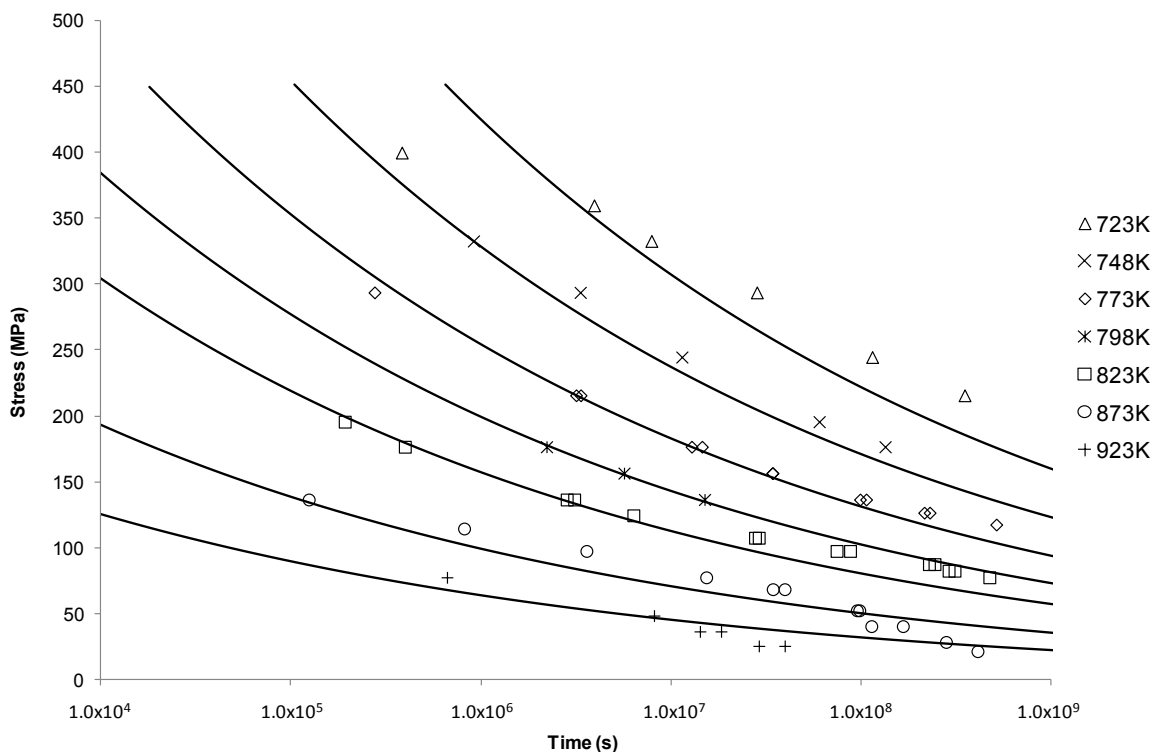
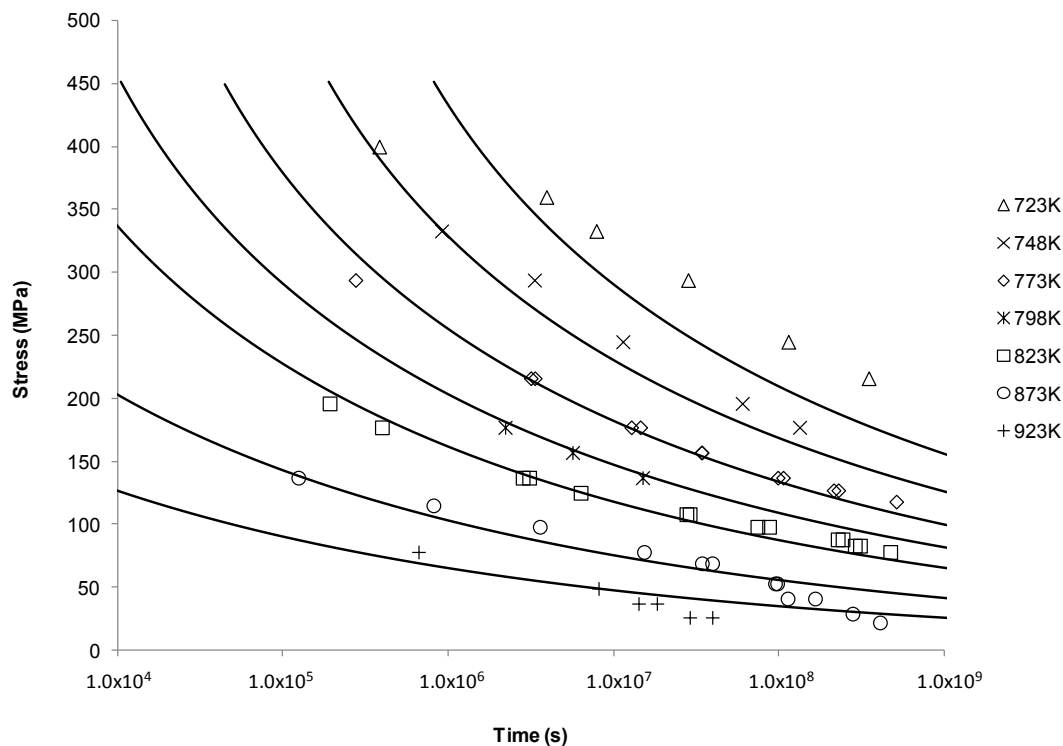


**Figure 8.** The stress vs. time to fracture curves of Soviet Model 2 using Grade 22 Steel creep data.



#### 4.3.7. The Minimum Commitment Approach

Figure 9 displays the results obtained from the Minimum Commitment approach. This method is a vast improvement upon the previous ones as it provides a better fit to the experimental data and more importantly reflects the trend of the data. This is seen through the change in the curve shape from the highest to the lowest temperature. This shift in the curve shape and consequential good prediction may be attributed to the increased flexibility and sensitivity of the approach gained from having a larger number of constants.

#### 4.3.8. The Hyperbolic-Tangent Approach

The alternative shape of stress-rupture curves produced by the hyperbolic tangent approach is evident in Figure 10. Using this approach, the constructed curves show reasonable fits to the observed creep behaviour as a result of the hyperbolic functions in its equation providing smooth curvatures. It is also observed that there is an inflection point at around 50%  $\sigma_{TS}$  at each corresponding temperature. This agrees with other observations [28–30] and implies that the creep mechanism is dependent on the applied stress level above and below  $\sigma_y$  (or  $\sigma_{TS}$ ). Another observation is that at intermediate temperatures (773, 823 and 873K) the curves deviate from the experimental data, in particular at the low stresses. This indicates that the shape of the outliers (highest and lowest temperature) dominate curve shapes and hence when using this method due care needs to be taken over the range of temperature it is applied to, and the amount of intermediate points included in the initial fitting of the constants.



**Figure 9.** The stress vs. time to fracture curves of the Minimum Commitment method using Grade 22 Steel creep data.

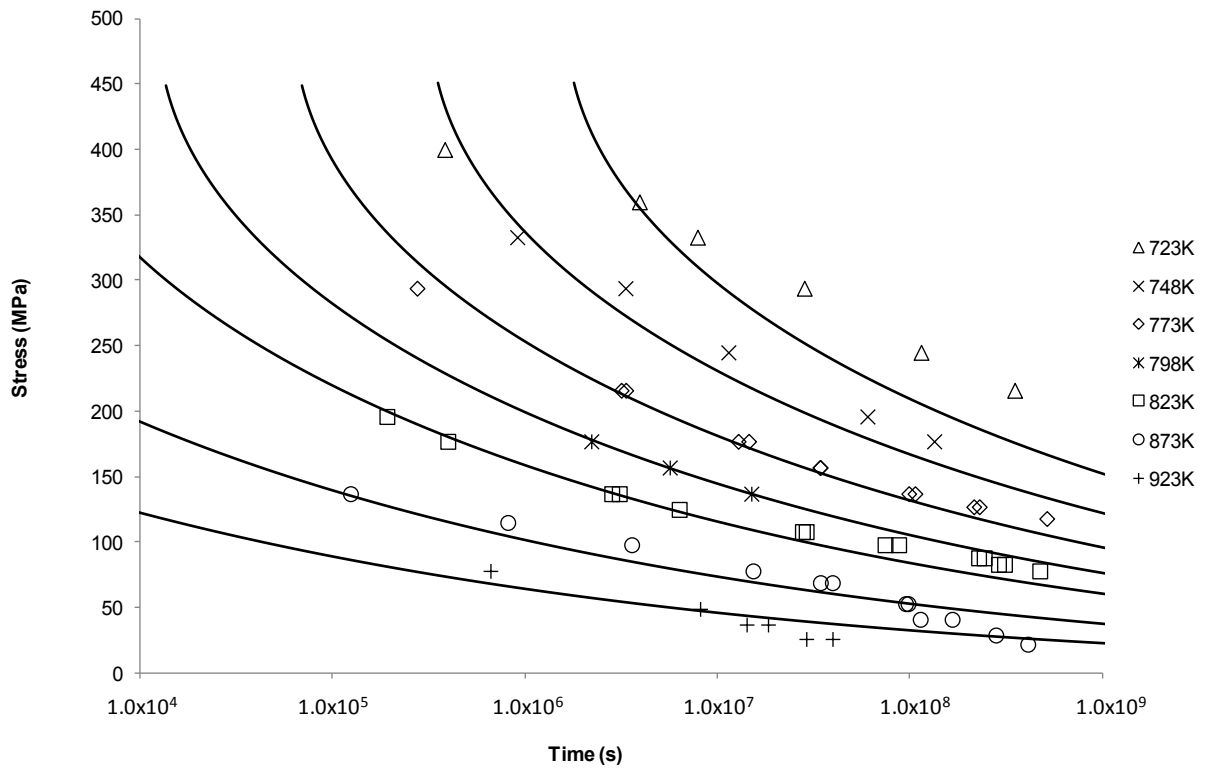
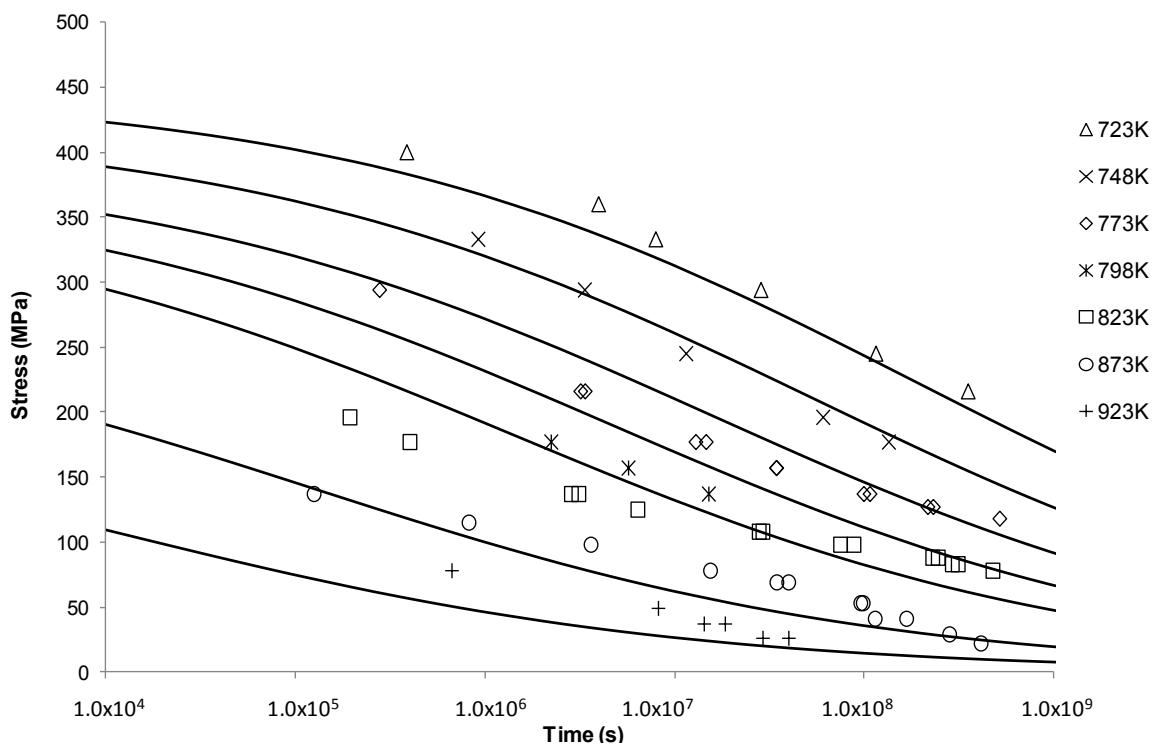


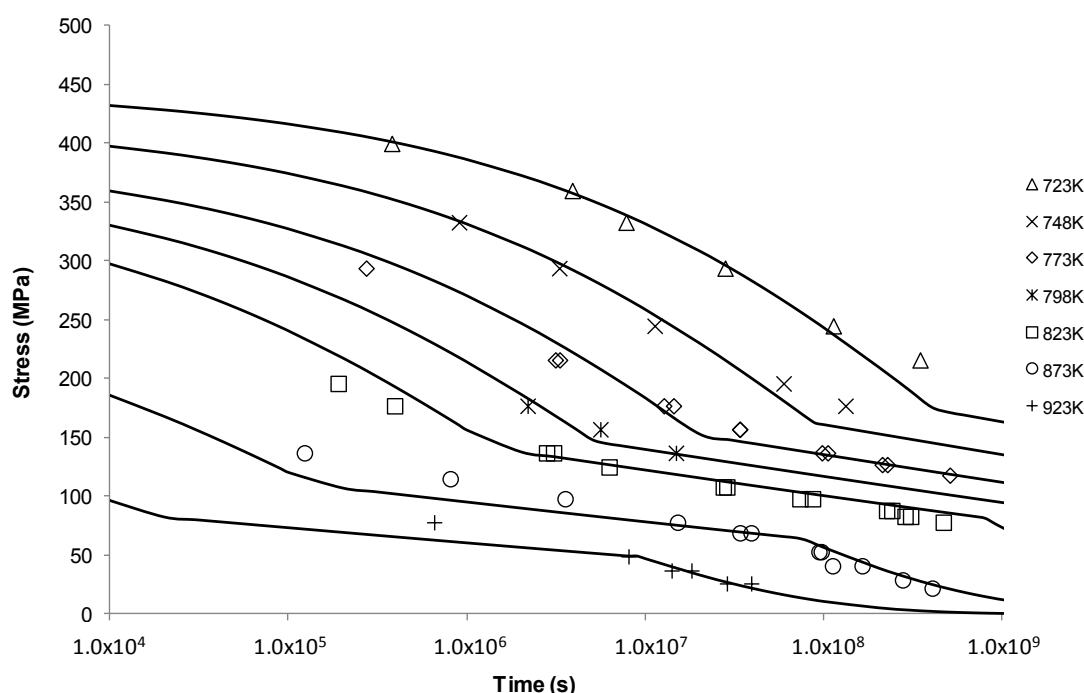
**Figure 10.** The Hyperbolic Tangent's stress vs. time to fracture predictive curves using Grade 22 Steel creep data.



### 4.3.9. The Wilshire Approach

Curves predicted by the Wilshire approach shown in Figure 11, are considered to be a good fit to the experimental measurements in both the high and the low stress regimes at all temperatures. It can also be observed from these curves that there are “kink” points at which the trend of the creep data changed according to the stress level involved (and hence a change in the constants  $k_1$  and  $u$ ). In recent studies, it was found that these inflection points separate regions of different activation energies in different stress regimes [50] signifying the role deformation mechanisms have in determining creep behaviour.

**Figure 11.** The Wilshire Equation’s stress vs. time to fracture predictive curves using Grade 22 Steel creep data.



### 4.3.10. Errors and Accuracy

The accuracy of each of the above approaches in predicting creep was evaluated using a Mean Squared Error (MSE) method where the error is calculated by:

$$MSE = \frac{1}{n} \sum_{t=1}^n [t_{\text{actual}} - t_{\text{predicted}}]^2 \tag{26}$$

where  $t_{\text{actual}}$  and  $t_{\text{predicted}}$  are the experimental and predicted times to failure, respectively, and  $n$  is the number of the available data points. Error calculations shown in Figure 12 and in Table 1 were evaluated by taking the total number of error for all temperatures for each of the approaches. Whilst there are numerable approaches to error calculation, the MSE was considered the most applicable as it is an aggressive approach and it provides a simple and clear means to distinguish between the various approaches. In Figure 12 it can be seen that the simpler models return larger errors, whilst the more

complex ones such as the SM2, Hyperbolic Tangent and Wilshire better represent the material’s creep properties.

**Figure 12.** Error analysis of the conventional and modern predictive approaches.

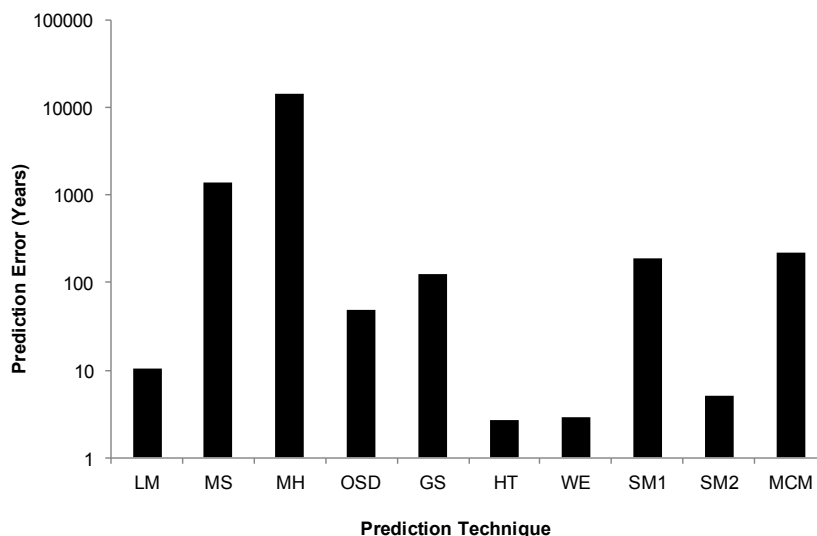


**Table 1.** Error values for the conventional and modern predictive approaches.

| Temperature (K) | Errors in each extrapolation technique (Years) |        |        |       |       |       |        |                    |         |       | Minimum Error |
|-----------------|--|--------|--------|-------|-------|-------|--------|--------------------|---------|-------|---------------|
|                 | LM   | MS     | MH     | OSD   | GS    | HT    | SM1    | SM2                | MCM     | WE    |               |
| 723             | 2.9406   | 3.783  | 3.819  | 1.824 | 4.03  | 1.541 | 3.0745 | 3.674              | 3.6367  | 2.425 | HT            |
| 748             | 0.657  | 1.243  | 0.67   | 0.095 | 1.007 | 0.582 | 0.8212 | 1.022              | 1.05086 | 1.072 | OSD           |
| 773             | 1.5671   | 3.171  | 356.3  | 1.489 | 25.46 | 2.038 | 2.7496 | 2.178              | 2.60138 | 0.376 | WE            |
| 798             | 0.1366   | 0.079  | 0.523  | 0.109 | 0.397 | 0.408 | 0.0051 | 0.035              | 0.02743 | 0.056 | SM1           |
| 823             | 1.0737   | 4.125  | 532.8  | 3.822 | 32.44 | 4.249 | 4.2348 | 3.284              | 3.63002 | 5.621 | LM            |
| 873             | 22.675   | 3006.4 | 30,968 | 108.1 | 274.2 | 2.819 | 407.24 | $1 \times 10^{-7}$ | 477.314 | 0.641 | SM2           |
| 923             | 0.4621   | 36.804 | 0.613  | 5.303 | 0.382 | 0.515 | 12.078 | 13.91              | 11.2147 | 0.145 | WE            |

Taking a closer look at Soviet Model 1 and Minimum Commitment approaches, these results should be expected. As highlighted when describing the approach, the Soviet and Minimum Commitment approaches rely on a large number of fitted constants meaning these equations have greater flexibility and sensitivity. Although this reproduces experimental data more accurately, it also means that these methods require greater care in application as the ability to produce unphysical curves or unreasonable constants is possible.

In considering the error associated with the two best methods, Hyperbolic Tangent and Wilshire, it is important to qualitatively and quantitatively consider each approach. The Hyperbolic Tangent approach provides a good fit to the creep-rupture data but from a visual inspection the region splitting Wilshire approach looks more accurate. The reason this is not reflected in the above error calculation is that the measurement of error is the difference in rupture times, which for the Wilshire approach produces an exaggerated error with higher temperatures due to the very flat nature of the curves produced. This limitation needs to be kept in mind when applying any creep lifing method as there are numerous ways to quantify error which may not reflect the quality of fit. In acknowledging these limitations, the Wilshire approach does not suffer the complexity of a large number of constants

requiring the determination of only two constants which have so far have proven to be constant, although the constants vary in different regimes. Therefore, from this treatment it can be seen that the more complex methods provide better results when predicting creep properties with the most promising methods for now being the Wilshire and Hyperbolic Tangent approaches due to their relative simplicity and prediction capability.

4.4. Approaches to Reproducing Full-Creep Curves (Titanium IMI834 Data)

4.4.1. The  $\theta$ -Projection Approach

The  $\theta$ -projection approach was examined using the available Titanium IMI834 data. A comparison is shown in Figures 13 and 14 for the 4- $\theta$  and 6- $\theta$  methods, respectively. It is evident from these figures that the 6- $\theta$  method is more capable of describing the whole creep curve, in particular, providing a more accurate description of primary creep. The limitation of this approach is that full creep curves need to be available prior to carrying out analysis using this approach.

Figure 13. Creep curve for 823 K, 600 MPa fitted using the 4- $\theta$  approach.

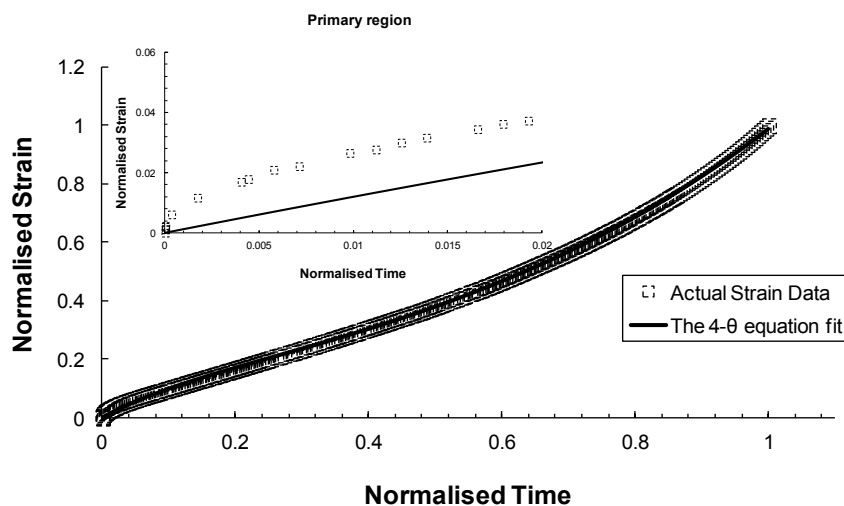
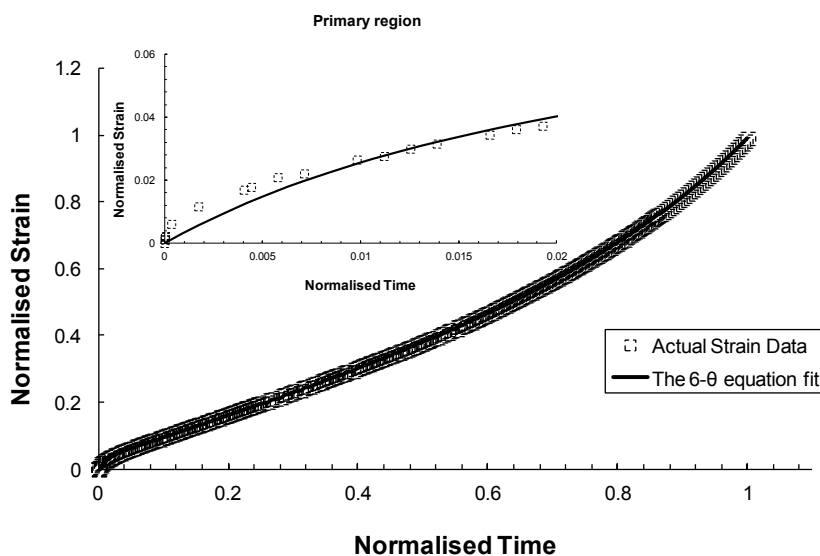


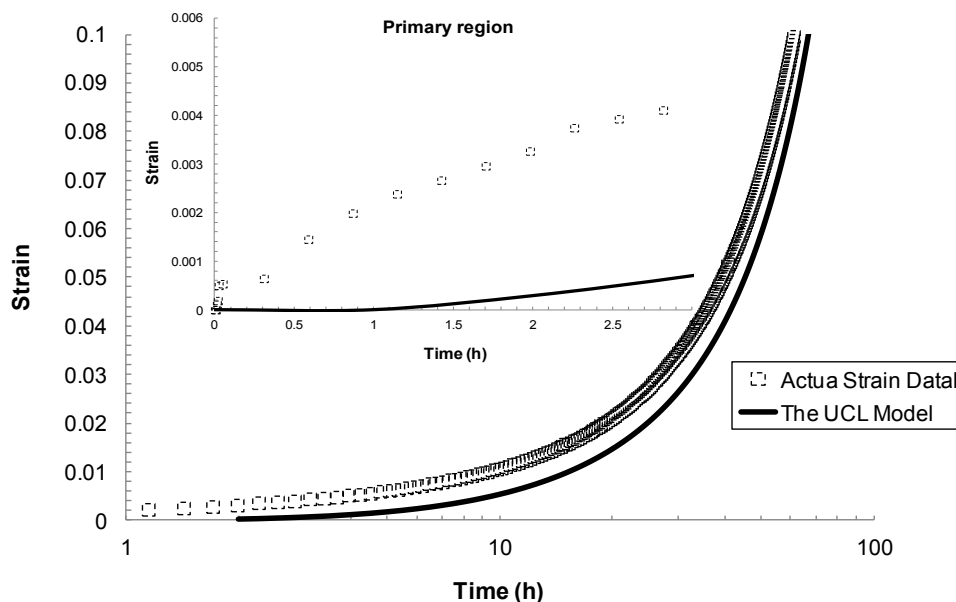
Figure 14. Creep curve for 823 K, 600 MPa fitted using the 6- $\theta$  approach.



#### 4.4.2. The Uniaxial Creep Lifting (UCL) Approach

The Uniaxial Creep Lifting approach is shown in Figure 15. From these results it can be seen that this approach was not able to accurately describe the primary creep region. This is not desirable for the aerospace industry as engineers are often faced with design problems that need to account for a material undergoing small strains.

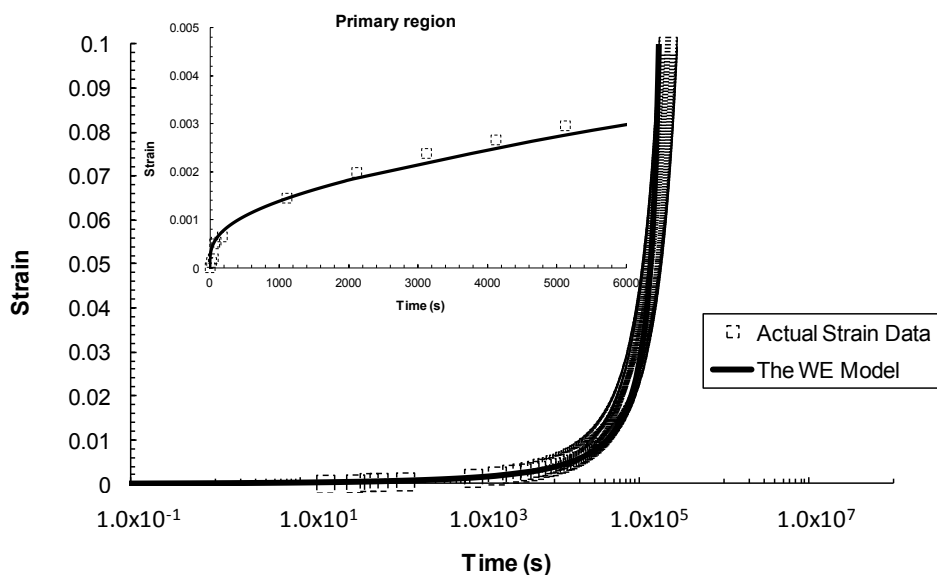
**Figure 15.** Creep curve for 923 K, 260 MPa predicted using the Uniaxial Creep Lifting approach.



#### 4.4.3. The Wilshire Approach

The Wilshire technique has provided an impressive description of the whole creep curve, as well as, the primary region as seen in Figure 16. This description of the creep process stands alone as the most accurate description of the previously discussed methods.

**Figure 16.** Creep curve for 923 K, 260 MPa predicted using the Wilshire approach.



Listed in Table 2 are the model equations used to fit the data for the creep rupture approaches used (Sections 4.3 and 4.4). In Table 3, the values of the constants for the various approaches are listed.

**Table 2.** Equations and parameters of creep life approaches.

| Creep Lifting Technique | Stress Function  | Note                           |
|-------------------------|--|--------------------------------|
| LM                      | $P_{LM} = -1.44 \times 10^{-6}\sigma^4 + 8.048 \times 10^{-4}\sigma^3 + 2.73 \times 10^{-2}\sigma^2 - 9.21 \times 10\sigma + 57175.13$   | constants explained in Table 3 |
| MH                      | $P_{MH} = 3.54 \times 10^{-11}\sigma^4 - 7.83 \times 10^{-8}\sigma^3 + 5.07 \times 10^{-5}\sigma^2 - 1.311 \times 10^{-2}\sigma + 1.464$ | constants explained in Table 3 |
| OSD                     | $\sigma = 4 \times 10^{-7} [(44250/T) - \log t]^{5.3787}$  | constants explained in Table 3 |
| MS                      | $\sigma = 4 \times 10^{19} [\log t + 0.0705T]^{-9.389}$  | constants explained in Table 3 |
| GS                      | $P_{GS} = -9.63 \times 10^{-6}\sigma^4 - 5.51 \times 10^{-3}\sigma^3 + 1.017 \times 10\sigma^2 - 3.65 \times 10^3\sigma + 5.609$         | constants explained in Table 3 |
| HT                      | $\sigma = \text{UTS}/2 (1 - \tanh[k \log(t/t_i)])$   | $k$ is constant                |
| WE                      | $\sigma/\text{UTS} = \exp(-k_1[t_r \exp(-Q_c^*/RT)]^u)$  | $u$ and $k_1 = f(\sigma)$      |
| SM1                     | $\log t = a + b \log T + c \log \sigma + d/T + f\sigma/T$  | constants explained in Table 3 |
| SM2                     | $\log t = a + b \log T + c(\log \sigma)/T + d\sigma/T + fT$  | constants explained in Table 3 |
| MCM                     | $\log t = a + b \log \sigma + c\sigma + d\sigma^2 + fT + g/T$  | constants explained in Table 3 |

**Table 3.** Determined constants of creep life approaches.

| Category                                   | Method  | Parameters   | Note  |
|--|---|--|---|
| Creep Lifting Techniques                   | LM  | $C_{LM} = 41.5$  | constant                                    |
|  | MH  | $\log t_a = -77.6$<br>$T_a = 986$  | constant                                    |
|  | OSD   | $C_{OSD} = 44250$  | constant                                    |
|  | MS  | $C_{MS} = 0.0705$  | constant                                    |
|  | GS  | $\log t_a = -48$<br>$1/T_a = 0.00093$  | constant                                    |
|  | HT  | $k = 0.144, t_i = \exp(-0.007T + 7.7992)$  | $t_i = f(T)$                                |
|  | SM1   | $a = 410.05, b = -53.734, c = -6.99, d = 4.68, f = -0.24$  | constants                                   |
|  | SM2   | $a = 560.26, b = -77.68, c = -7129.34, d = 8.3, f = 14363.1$   | constants                                   |
|  | MCM   | $a = 101.83, b = -6.47, c = -0.0139, d = 0.000027,$<br>$f = -0.065, g = 2.0097$  | constants                                   |
|  | WE  | Low stress regime: $u = 0.2944, k_1 = 624$<br>Intermediate stress regime: $u = 0.0714, k_1 = 6.45$<br>High stress regime: $u = 0.3072, k_1 = 3584$       | $u$ and $k_1 = f(\sigma)$                   |
| Full creep representation (923 K/ 260 MPa) | $\theta$ -projection                          | 4- $\theta$ method: $\theta_1 = 0.9244, \theta_2 = 0.3118, \theta_3 = 0.0162, \theta_4 = 3.833$  | $\theta = f(\sigma, T)$                     |
|  |   | 6- $\theta$ method: $\theta_1 = 30.00021, \theta_2 = 0.00966, \theta_3 = 0.01297,$<br>$\theta_4 = 3.99825, \theta_5 = 0.00064, \theta_6 = 1000.284$      |   |
|  | WE  | Low stress regime: $w = 0.21, k_3 = (3.815484/\epsilon^{0.8}) + 350$<br>High stress regime: $w = 0.8, k_3 = (3 \times 10^9/\epsilon) + 2 \times 10^{10}$ | $w = \text{constant},$<br>$k = f(\epsilon)$ |
| UCL  | $k = 0.000695, t_{tr} = 3.34069, M' = 31.092$ | $k, t_{tr},$ and<br>$M' = f(\sigma)$   |   |

## 5. Discussion and Conclusions

The requirement for reliable methods of predicting long-term creep behaviour is more critical now than it has ever been. With conventional power plant building still widespread, the opportunity to increase operating temperatures and/or reduce material costs through higher stresses, is highly desirable but unrealised. One of the reasons for this is that there is little confidence in creep prediction on the timescales required for industrial applications without extensive and protracted testing.

The limitations of traditional power law based approaches have long been recognised [51] although designers have been reticent to move away from these approaches due to their simplicity and ease of use. Presumably, this is also because no alternative approach offers a significant enough increase in confidence to warrant a change in creep behaviour prediction and characterisation methodology. The Larson-Miller approach shown in Figure 2 aptly demonstrates the nature of the problem. Fits based on rupture data seem reasonable for lower temperatures and the behaviour of the material is well described. However, for higher temperatures the accuracy of the fits decreases markedly and non-conservative predictions of rupture time occur. Obviously this presents a significant problem and results in the undesired need for further testing.

Looking at the next generation of creep lifing approaches provides no better alternative to the Larson-Miller approach. This is evident from the Manson-Haferd approach providing poor fits at the highest and lowest temperatures, the Orr-Sherby-Dorn approach fitting poorly at short lifetimes and high temperatures, the Manson-Succop approach fitting poorly at the temperature extremes and short lifetimes, and the Goldhoff-Sherby approach fitting poorly at low temperature and short lifetime. To try and overcome this, more complex models were developed. The Soviet Prediction approach offers better fits, but has very limited extrapolation ability and inherits complexity due to the number of constants that need to be fitted. The Minimum Commitment approach offers good fits but still suffers the need to fit a large number of constants to sample data.

Regaining simplicity in implementation by reduction of constants, both the Hyperbolic Tangent and Wilshire approaches provide good fits with minimum associated complexity. For the Hyperbolic Tangent approach developed by Rolls-Royce plc, the creep curves trend to  $\sigma_{TS}$  for each temperature as  $t \rightarrow 0$ , and trend to an infinite life as  $\sigma \rightarrow 0$ . This represents the expected physical behaviour of the material under such conditions. As such, the Hyperbolic Tangent approach has been applied to a number of materials [30] and clearly offers a step forward in prediction of creep. However, the complex behaviour of Grade 22 steel provides problems which the technique is unable to accommodate, seen by poor prediction of long rupture times between 773 and 873 K. Despite the fact that the Hyperbolic Tangent approach produces the lowest MSE in comparison to the Wilshire approach, it is clear that the changing trends in the creep-rupture data are not always accommodated. The issue here is that the Hyperbolic Tangent approach offers a point of inflection at  $\sigma = 0.5\sigma_{TS}$ , which presumably is not offering enough flexibility in the curve shape to accommodate the behavior of the material in question.

The Wilshire equations share a number of common features with the Hyperbolic Tangent approach including providing good fits to experimental creep data. One of the common features between approaches is stress normalisation and the creep curve trending towards infinite life as  $\sigma \rightarrow 0$ . Key publications have sought to rationalise the assumptions made when using the equations, and in particular the behaviour of materials considered [8,16,31,32]. Whilst normalisation by  $\sigma_{TS}$  is particularly useful in

reducing batch to batch scatter, perhaps the most important element in applying the equations is the ability of this approach to “react” to creep mechanism regimes as shown in Figure 11. It is apparent that the first “transition” (change in  $k_1$  and  $u$ ), occurs at the yield stress of the material. This change in behaviour is perhaps unsurprising due to changes in dislocation behaviour which occur above and below the yield stress. Below the yield stress creep occurs through the movement of pre-existing dislocations and mainly by grain boundary zone deformation. Above the yield stress, new dislocations are continuously generated which is often noticeable by a more extended primary phase that is limited only by exhaustion when strain hardening offsets dislocation generation. As this decaying process is offset by an accelerating tertiary phase, which is brought about by damage such as cavitation and triple point cracking, a minimum rather than secondary creep rate occurs. Previous studies have inferred these mechanisms from changes in elongation and reduction in area measurements of creep tests above and below yield [52]. The second transition occurs at high temperature, *i.e.*, 798–923 K, and relatively long rupture times is due to degradation of the material through overaging. The bainitic structure evident prior to testing begins to break down and the microstructure evolves to ferrite with coarse molybdenum carbide particles. Interestingly, activation energies calculated using the Wilshire approach well represents these changes in behaviour. Above the yield stress, creep occurs within the grains and the activation energy calculated for creep is  $280 \text{ kJ}\cdot\text{mol}^{-1}$ , approximately the value for self diffusion in the ferrite lattice. Below the yield stress, the value drops to  $230 \text{ kJ}\cdot\text{mol}^{-1}$  as deformation is confined to the grain boundary zones. However, the activation energy for low stresses/high temperatures returns to  $280 \text{ kJ}\cdot\text{mol}^{-1}$ , as following the degradation of bainite to ferrite, creep returns to grain interiors in this effectively weaker material [8].

When considering the MSE error analysis for predicted creep life alongside the criteria provided by the ECCC, it is clear from both Figure 12 and Table 1, that the Wilshire and hyperbolic Tangent approaches provide the most accurate fits overall with the Wilshire Equations being most accurate for a number of temperatures. Interestingly, unlike the power law methods, the curve shape produced by the Wilshire is not its most significant advantage. Rather, the ability of the approach to react to creep mechanism changes which have been observed, offers a greater advantage as the underlying physical phenomena are represented within the approach. The effectiveness of this technique in predicting 100,000 h creep life based on only 5000 h has been demonstrated for a number of alloys [8,53]. It should also be noted here that the “region splitting” technique (transition) utilised in the Wilshire approach is not a wholly original approach with previous examples, particularly by Kimura *et al.* [54], worth consideration.

In summarizing the full creep curve approaches, we can see a greater emphasis on representing the underlying physical processes of creep. The most established of these methods is  $\theta$ -Projection which relies on extrapolating from known curves to unknown curves with dependence on the same physical phenomena being present in both cases. The additional term in the 6- $\theta$  approach provided a better description of the primary creep than compared to the 4- $\theta$ . Taking a more fundamental route, the Uniaxial Creep Lifting approach is mechanistically-based and represents a group of models that try to encompass the underlying physical process of creep. In literature, replication of creep curves via this approach has been reasonable even though in this review the method poorly predicted the primary phase of the creep curve [39]. Wilshire offers an additional approach that lies between the  $\theta$ -Projection and the Uniaxial Creep Lifting methods. The Wilshire approach, as previously discussed, is a model



that is sympathetic to the underlying creep mechanism without explicitly defining it. As such, it is a combination of a physically independent and a mechanistically-defined model which produces good, if not better, fits than the other approaches reviewed here.

In considering the requirements of the aerospace and power generation industries, the approaches reviewed here provide a summary of the past and an insight into the future. Implementing power law-based creep methods in the modern world is becoming harder to justify with greater computing power available to deal with more complex accurate models such as the Hyperbolic-Tangent, Soviet, Minimum Commitment and the Wilshire approaches. For the whole creep curve prediction, it can be seen that incorporating the underlying physical phenomena is producing more accurate models that encapsulate and enhance our understanding of the processes materials experience. Clearly, collaboration within the community would offer opportunities for further development of these approaches and as such bring closer to realisation the goal of a comprehensive creep behavior model.

### Acknowledgments

This research was carried out as part of a strategic partnership between Swansea University, the Engineering and Physical Sciences Research Council (EPSRC) and Rolls-Royce plc. The financial support from EPSRC and Rolls-Royce plc is greatly appreciated.

### Author Contributions

The cooperative work between all authors facilitated the publication of this paper in its final format. In this regard, Zakaria Abdallah conducted the research, applied the various methods and wrote the paper. Veronica Gray provided detailed expertise regarding the fitting of parameters. Mark Whittaker provided interpretation of the behaviour of Grade 22 steels and the Wilshire Equations. Karen Perkins provided expertise on curve fitting methodologies.

### Conflicts of Interest

The authors declare no conflict of interest.

### References

1. Wilshire, B.; Evans, R.W. *Introduction to Creep*; the Institute of Materials: London, UK, 1993.
2. Cane, B.J.; Aplin, P.F. Creep life assessment methods. *J. Strain Anal. Eng. Design* **1994**, *29*, 225–232.
3. Allen, D.; Garwood, S. *Energy Materials-Strategic Research Agenda*; Materials UK Energy Review 2007. Available online: [http://www.matuk.co.uk/docs/1\\_StrategicResearchAgenda%20FINAL.pdf](http://www.matuk.co.uk/docs/1_StrategicResearchAgenda%20FINAL.pdf) (accessed on 23 April 2014).
4. National Institute for Materials Science (NIMS). *Data Sheets on the Elevated Temperature Properties of 2.25Cr-1Mo Steel for Boiler and Heat Exchanger Seamless Tubes (STBA 24)*; National Institute for Materials Science: Ibaraki, Japan.
5. Holdsworth, S.R.; Merckling, G. ECCC Developments in the assessment of Creep-Rupture Data. In Proceedings of the Sixth International Charles Parsons Conference on Engineering Issues in Turbine Machinery, Power Plant and Renewables, Trinity College, Dublin, Ireland, 16–18 September 2003.

6. BS PD 6605. *Guidance on Methodology for Assessment of Stress-Rupture Data*; British Standard Institution: London, UK, 1998.
7. Brown, S.G.; Evans, R.W.; Wilshire, B. Creep strain and creep life prediction for the cast nickel-based superalloy IN-100. *Mater. Sci. Eng.* **1986**, *84*, 147–156.
8. Whittaker, M.; Wilshire, B. Advanced procedures for long-term creep data prediction for 2.25 chromium steels. *Metall. Mater. Trans. A* **2013**, *44*, 136–153.
9. Larson, F.R.; Miller, J. A time-temperature relationship for rupture and creep stresses. *Trans. ASME* **1952**, *74*, 765–775.
10. Kaufman, J.G.; Long, Z.; Ningileri, S. Application of time-temperature-stress parameters to high temperature performance of aluminium alloys. In *Aluminum Alloys for Transportation, Packaging, Aerospace, and Other Applications*; Das, S.K., Yin, W., Eds.; Book News, Inc., Portland, OR, USA, 2007; pp. 137–146.
11. Larke, E.C.; Inglis, N.P. A critical examination of some methods of analysing and extrapolating stress-rupture data. In Proceedings of the Institution of Mechanical Engineers, Conference Proceedings, London, UK, 1 June 1963; Volume 178, pp. 33–47.
12. Manson, S.S.; Haferd, A.M. *A Linear Time-Temperature Relation for Extrapolation of Creep and Stress-Rupture Data*; National Advisory Committee for Aeronautics (NACA): Washington, DC, USA, 1953.
13. Penny, R.K.; Marriott, D.L. *Design for Creep*, 2nd ed.; Chapman & Hall: London, UK, 1995.
14. Murry, G. Extrapolation of the Results of Creep Tests by Means of Parametric Formulae. In Proceedings of the Institution of Mechanical Engineers, London, UK, 1 June 1963; Volume 178, pp. 87–203.
15. Orr, R.; Sherby, O.; Dorn, J. Correlation of rupture data for metals at elevated temperatures. *Trans. ASM* **1954**, *46*, 113–118.
16. Wilshire, B.; Scharning, P.J. A new methodology for analysis of creep and creep fracture data for 9%–12% chromium steels. *Int. Mater. Rev.* **2008**, *53*, 91–104.
17. Carreker, R. Plastic flow of platinum wires. *J. Appl. Phys.* **1950**, *21*, 1289–1296.
18. Murray, J.D.; Truman, R.J. The High Temperature Properties of Cr-Ni-Nb and Cr-Ni-Mo Austenitic Steels. In Proceedings of the Institution of Mechanical Engineers, Conference Proceedings, London, UK, 1 June 1963; Volume 178, pp. 55–67.
19. Manson, S.; Succop, G. *Stress-Rupture Properties of Inconel 700 and Correlation on the Basis of Several Time-Temperature Parameters, 1956*; ASTM Special Technical Publication (No. 174); ASTM: West Conshohocken, PA, USA; p. 40.
20. Zharkova, N.; Botvina, L. Estimate of the life of a material under creep conditions in the phase transition theory. *Doklady Phys.* **2003**, *48*, 379–381.
21. Goldhoff, R.; Hahn, G. Correlation and Extrapolation of Creep-Rupture Data of Several Steels and Superalloys Using Time-Temperature Parameters. In *ASM Publication D-8-100*; American Society for Metals, Ed.; American Society for Metals: Cleveland, OH, USA, 1968; pp. 199–247.
22. Evans, M. Method for improving parametric creep rupture life of 2.25Cr-1Mo steel using artificial neural networks. *Mater. Sci. Technol.* **1999**, *15*, 647–658.
23. Trunin, I.I.; Golubova, N.G.; Loginov, E.A. New Method of the Extrapolation of Creep-Test and Long-Time Strength Results. In Proceedings of the 4th International Symposium on Heat-Resistant Metallic Materials, Mala Fatra, Czechoslovakia, 1971; pp. 168–176.

24. British Standards Institute. *PD 6605-1:1998, Guidance on Methodology for Assessment of Stress-Rupture Data. Procedure for Derivation of Strength Values*; British Standards Institute: London, UK, 1998.
25. Manson, S.S.; Ensign, C.R. Interpolation and Extrapolation of Creep Rupture Data by the Minimum Commitment Method. In Proceedings of the Part I, Focal Point Convergence. Pressure Vessel & Piping Conference, Montreal, QC, Canada, 26–29 June 1978; pp. 299–398.
26. Manson, S.S.; Ensign, C.R. *A Specialised Model for Analysis of Creep-Rupture Data by the Minimum Commitment*; Station-Function Approach, NASA TM-X-52999; National Aeronautics and Space Administration (NASA): Washington, DC, USA, 1971.
27. Ding, J.; Kenneth, C.; Brinkman, C. A Comparative Study of Existing and Newly Proposed Models for Creep Deformation and Life Prediction of Si<sub>3</sub>N<sub>4</sub>. In *Life Prediction Methodologies and Data for Ceramic Materials*; Brinkman, C.R., Duffy, S.F., Eds.; ASTM International: West Conshohocken, PA, USA, 1994; pp. 62–83.
28. Williams, S.J. *An Automatic Technique for the Analysis of Stress Rupture Data*, Report MFR30017; Rolls-Royce plc: Derby, UK, 1993.
29. Williams, S.J. The Implementation of Creep Data in Component FE Analyse. In Proceedings of the 1st International Conference on Component Optimisation, Swansea, UK, 29 March–1 April 1999; pp. 139–146.
30. Williams, S.J.; Bache, M.R.; Wilshire, B. Recent developments in the analysis of high temperature creep and creep fracture behaviour. *Mater. Sci. Technol.* **2010**, *26*, 1332–1337.
31. Wilshire, B.; Scharning, P.J. Prediction of long-term creep data for forged 1Cr-1Mo-0.25V steel. *Mater. Sci. Technol.* **2008**, *24*, 1–9.
32. Wilshire, B.; Battenbough, A. Creep and creep fracture of polycrystalline copper. *Mater. Sci. Eng. A* **2007**, *443*, 156–166.
33. Holdsworth, S. The European Creep Collaborative Committee (ECCC) approach to creep data assessment. *J. Press. Vessel Technol.* **2008**, *130*, 024001:1–024001:6.
34. Tancret, F.; Sourmail, T.; Yescas, M.A.; Evans, R.W.; McAleese, C.; Singh, L.; Smeeton, T.; Bhadeshia, H.K.D.H. Design of a creep resistant nickel-base superalloy for power plant applications: Part 3 (experimental results). *Mater. Sci. Technol.* **2003**, *19*, 296–302.
35. Evans, M. Sensitivity of the theta projection technique to the functional form of the theta interpolation/extrapolation function. *J. Mater. Sci.* **2002**, *37*, 2871–2884.
36. Evans, R.W.; Scharning, P.J. The theta projection method applied to small strain creep of commercial aluminum alloy. *Mater. Sci. Technol.* **2001**, *17*, 487–493.
37. Evans, R.W. Wilshire, B. The role of grain-boundary cavities during tertiary creep. In *Creep and Fracture of Engineering Materials and Structures*; Wilshire, B., Owen, D.R.J., Eds.; Pineridge Press: Swansea, UK, 1981; pp. 303–314.
38. Evans, R.W. The theta projection method and low creep ductility materials. *Mater. Sci. Technol.* **2000**, *16*, 6–8.
39. Wu, X. *Uniaxial Creep Lifing Methodology-II: Creep Modeling for Waspaloy and Udimet 720Li*; Report No. LTR-SMPL-2010-0156; National Research Council (NRC): Montreal, QC, Canada.
40. Abdallah, Z.; Perkins, K.; Williams, S. Advances in the Wilshire technique—Full creep curve representation for the aerospace alloy titanium 83. *Mater. Sci. Eng. A* **2012**, *550*, 176–182.

41. Evans, R.W.; Little, E.A.; Preston, J.A.; Wilshire, B. Rationalisation of the Creep Behaviour of Oxide-Dispersion-Strengthened Alloys. In Proceedings of the Fifth International Conference on Creep and Fracture of Engineering Materials and Structures, Swansea, UK, 28 March–2 April 1993; Institute of Materials: Swansea, UK; p. 812.
42. Wilshire, B.; Burt, H. Long-term creep design data for forged 1Cr-1Mo-0.25V steel. *J. Strength Fract. Complex.* **2006**, *4*, 65–73.
43. International Organization for Standardization (ISO). *Metallic Materials—Uniaxial Creep Testing in Tension—Method of Test*; ISO 204:2009; ISO: Geneva, Switzerland, 2009.
44. *Titanium and Titanium Alloys: Fundamentals and Applications*; Leyens, C., Peters, M., Eds.; Wiley-VCH: Weinheim, Germany, 2003.
45. Krivenyuk, V.; Mamuzic, I. Correlation of creep-rupture data for complex alloys at elevated temperatures. *Metalurgija* **2007**, *46*, 79–85.
46. Cipolla, L.; Gabrel, J. New Creep Rupture Assessment of Grade 91. In Proceedings of the ETD Conference: Industry and Research Experience in the Use of P/T91 in HRSGS/Boilers, IOM3, London, UK, 7–8 December, 2005.
47. Samuel, K.G.; Ray, S.K. Larson–Miller correlation for the effect of thermal ageing on the yield strength of a cold worked 15Cr-15Ni-Ti modified austenitic stainless steel. *Int. J. Press. Vessels Pip.* **2006**, *83*, 405–408.
48. Kinzoku Zairyō Gijutsu Kenkyūjo. *Data Sheets on the Elevated-Temperature Properties of 1Cr-1Mo-0.25V Steel Castings for Steam Turbine Casings (ASTM A356/A356M-9), No. 31B*; National Research Institute for Metals (NRIM): Tokyo, Japan, 1994.
49. Kinzoku Zairyō Gijutsu Kenkyūjo. *Data Sheets on the Elevated-Temperature Properties of Centrifugally Cast 25Cr-20Ni-0.4C Steel Tubes for Use in Reformer Furnaces (SCH 22-CF), No. 16B*; National Research Institute for Metals (NRIM): Tokyo, Japan, 1990.
50. Wilshire, B.; Whittaker, M. The role of grain boundaries in creep strain accumulation. *Acta Mater.* **2009**, *57*, 4115–4124.
51. Whittaker, M.; Wilshire, B. Creep and creep fracture of 2.25Cr–1.6W steels (Grade 23). *Mater. Sci. Eng. A* **2010**, *527*, 4932–4938.
52. Whittaker, M.; Evans, M.; Wilshire, B. Long-term creep data prediction for type 316H stainless steel. *Mater. Sci. Eng. A* **2012**, *552*, 145–150.
53. Whittaker, M.; Wilshire, B.; Brear, J. Creep fracture of the centrifugally-cast super austenitic steels: HK40 and HP40. *Mater. Sci. Eng. A* **2013**, *580*, 391–396.
54. Kimura, K.; Sawada, K.; Kushima, H. Influence of Stress on Creep Deformation Properties of 9.12Cr Ferritic Creep Resistant Steels. In Proceedings of the 34th MPA-Seminar and VGB-Symposium, Materials and Components Behaviour in Energy & Plant Technology, Stuttgart, Germany, 9–10 October 2008.